Electron collisions with NO: Elastic scattering, vibrational excitation, and $^2\Pi_{1/2} \rightleftharpoons {}^2\Pi_{3/2}$ transitions

Michael Allan

Department of Chemistry, University of Fribourg, Switzerland

Abstract. Absolute differential elastic and vibrational excitation cross sections have been measured for NO at 135° with resolution of the $^2\Pi_{1/2}$ and $^2\Pi_{3/2}$ spin-orbit components of the ground electronic term. The electronic fine structure excitation is dominated by the $^3\Sigma^-$ and the $^1\Delta$ resonances of NO^-, the nonresonant contribution is very small. The cross section is very large, it has about the same magnitude as the resonant part of the elastic cross section. The magnitudes and shapes of the vibrational cross sections are essentially independent of whether the electronic fine structure transition is simultaneously excited or not. The vibrational cross sections have structures with interesting irregular shapes. Relative cross sections have been also measured at 180° and show differences in intensities of the resonant structures above 1.6 eV.

PACS numbers: 34.80.Gs

1. Introduction

The knowledge of the interactions of slow electrons with nitric oxide is important because NO is used as a plasma gas. Moreover, it has an unpaired electron and a $^2\Pi$ ground electronic term [1, 2] and thus offers an opportunity to study electron collisions with radicals, and in particular the excitation of the electronic fine structure transitions [3]. The present work employs the improved resolution and low energy capacity of the electron spectrometer [4] used in the previous study to investigate in more detail the elastic scattering and vibrational excitation, both pure and accompanied by the electronic fine structure transitions.

There are numerous electron collision studies on NO which do not distinguish the two spin-orbit components. The elastic scattering study of Ehrhardt and Willmann [5], the transmission study of Boness *et al* [6], and the trapped electron study of Spence and Schulz [7] revealed sharp structures due to the $^3\Sigma^-$ resonance of NO^-. Burrow [8] measured the derivative of the elastic cross section at 180° and detected the origin of the $^1\Delta$ resonance at $0.65-0.75$ eV. Zecca *et al* [9] measured the total absolute cross section. Tronc *et al* [10] measured differential ($40°-115°$) elastic and vibrational excitation (up to $v = 5$) cross sections with 50 meV resolution. Teillet-Billy and Fiquet-Fayard [11] used the results of Tronc *et al* to calculate the internuclear separation and autodetachment lifetimes of NO^-. They also calculated the vibrational excitation cross sections *via* the $^1\Delta$ resonance. Absolute differential elastic and vibrational excitation cross sections have been measured from 1.5 to 40 eV and from 10° to 130° by Mojarrabi *et al* [12]. The study has recently been extended to lower energies by Jelisavcić *et al* [13]. Total integral cross sections have been measured by the time-of-flight method by Alle *et al* [14] and Buckman *et al* [15]. Randell *et al* [16] studied the resonances at low energies in NO cooled by supersonic expansion. Josić *et al* [17] derived vibrational cross sections from swarm parameters. Zecca *et al* [18] made a comparative study of the various data sets. Tennyson and Noble [19] calculated the resonance parameters for the low-lying states of NO^- using the R-matrix method. Zhang *et al* [20] recently reported an *ab initio* calculation of the elastic and vibrational excitation cross sections. Photodetachment studies [21, 22] determined the electron affinity, the latter study yielding the value of 0.026 ± 0.005 eV, together with an independent value for the NO^- internuclear separation $r_e(NO^-) = 1.271 \pm 0.005$ Å.

2. Experiment

The measurements were performed using a spectrometer with hemispherical analyzers [4, 23]. The energy resolution was about 10 meV in the energy-loss mode, corresponding to about 7 meV in the incident electron beam, at a beam current of around 40 pA. The energy of the incident beam was calibrated on the 19.365 eV [24] ^{2}S resonance in helium and is accurate to within ±10 meV. The analyzer response function was determined by recording the elastic signal in helium and comparing it to the calculated cross section

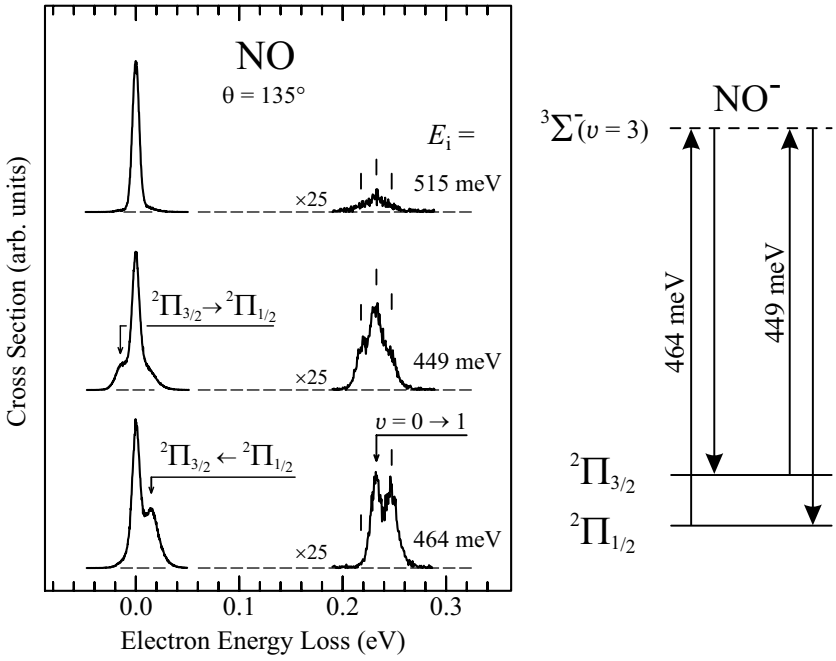

Figure 1. Electron energy loss spectra of NO (left) and a schematic diagram of the spin-orbit states of neutral NO and the $v' = 3$ level of the NO^- $^3\Sigma^-$ resonance.

[25]. The same response function was also used to correct the inelastic cross sections. This procedure can not be used below about 0.1 eV because of the falling incident beam current. The response function was therefore assumed to be flat below 0.1 eV. The correctness of this assumption was verified by recording the vibrational excitation cross sections of CO_2 near threshold. The cross sections within the first 0.1 eV above threshold are less accurate than at higher energies, however. NO was introduced through a 0.25 mm diameter effusive nozzle kept at ∼30°C. The backing pressure was 1.1 mbars for all measurements except those determining the absolute value, which were performed with a backing pressure of around 0.1 mbars. Absolute values of the cross sections were determined by comparison with the theoretical helium elastic cross section [25], using the relative flow method, and are accurate within about ±25%.

3. Results and Discussion

Figure 1 shows energy loss spectra of NO. The shapes of the spectra depend sensitively on the incident energy, indicating a pronounced effect of resonances. The incident energy in the bottom spectrum in figure 1 is chosen such as to reach the $v = 3$ level of the NO^- $^3\Sigma^-$ resonance from the ground $^2\Pi_{1/2}$ state, and the spin-orbit *inelastic* transition is pronounced, both pure and superimposed on the $v = 0 \rightarrow 1$ vibrational transition. The spin-orbit *superelastic* transition is nearly absent at this incident energy, because the resonance cannot be reached from the excited $^2\Pi_{3/2}$ state. The superelastic transition is pronounced at the slightly lower incident energy of 449 meV, adequate to reach the

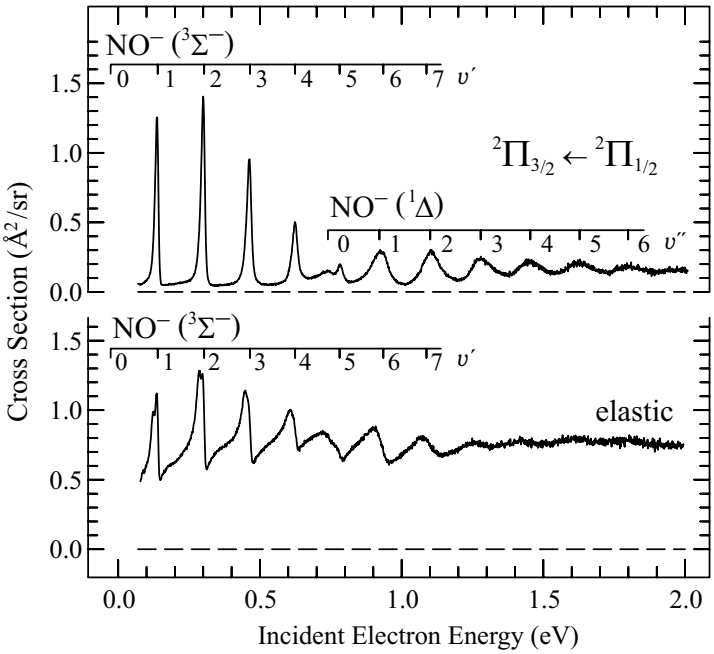

Figure 2. Differential elastic cross section $\langle\sigma_{\Delta\Omega=0}\rangle$ (bottom), and cross section for electronic fine structure excitation $\sigma_{\Delta\Omega=+1}$. The scattering angle was $\theta = 135°$.

resonance from the upper spin-orbit state. The topmost curve in figure 1 shows that both spin-orbit and vibrational transitions are weak with an incident energy off resonance.

The thermal populations of the $\Omega = 1/2$ and $\Omega = 3/2$ states are 0.64 and 0.36 in the current experiment [3]. The signals where Ω does not change, that is, the elastic peak at $\Delta E = 0$, and the pure $v = 0 \rightarrow 1$ peak at $\Delta E = 0.233$ eV, are the sum of the signals from NO in the $\Omega = 1/2$ and $3/2$ states. In contrast, signals where Ω does change stem from one or the other initial state. This puts some restrictions on which cross sections can be determined from the data. The cross sections where Ω does not change are an average over the thermal populations of the $\Omega = 1/2$ and $3/2$ states. The averaging will be expressed by angle brackets, for example $\langle\sigma_{\Delta\Omega=0}\rangle$ for the vibrationally elastic cross section, and $\langle\sigma^{v=0\rightarrow1}_{\Delta\Omega=0}\rangle$ for the excitation of one vibrational quantum. These cross sections can be expressed as, for example, $\langle\sigma_{\Delta\Omega=0}\rangle = 0.64\cdot\sigma_{\Omega=1/2\rightarrow1/2} + 0.36\cdot\sigma_{\Omega=3/2\rightarrow3/2}$, but the individual 'Ω-pure' cross sections are not measurable in the present experiment except near a narrow resonant structure as explained below.

The cross sections where Ω does change are not averages but refer to a state with a given Ω and will be designed as $\sigma_{\Omega=1/2\rightarrow3/2}$ and $\sigma_{\Omega=3/2\rightarrow1/2}$ (or $\sigma_{\Delta\Omega=+1}$ and $\sigma_{\Omega=-1}$ for brevity) for the vibrationally elastic cross section, $\sigma^{v=0\rightarrow1}_{\Delta\Omega=+1}$ and $\sigma^{v=0\rightarrow1}_{\Omega=-1}$ etc., for vibrational excitation. Cross sections summed over all $\Delta\Omega$ transitions and averaged over the thermal populations were constructed from the measured data in some cases, for example, $\langle\sigma_{\Delta\Omega=0,\pm1}\rangle = \langle\sigma_{\Delta\Omega=0}\rangle + 0.64\cdot\sigma_{\Delta\Omega=+1} + 0.36\cdot\sigma_{\Delta\Omega=-1}$. These summed cross sections can be compared to results of experiments which do not resolve the individual $\Delta\Omega$ transitions or to theory which does not take the spin-orbit splitting into account.

Table 1. Absolute differential elastic cross sections $\langle\sigma_{\Delta\Omega=0}\rangle$ measured at $\theta = 135°$ using the relative flow method.

Energy (eV)	Cross Section (Å^2/sr)
0.2	0.54
0.6	0.83
1.2	0.65

Needless to say, all cross sections are averaged over the rotational transitions.

The absolute differential elastic cross sections given in table 1 were measured using the relative flow method at three discrete electron energies of 0.2, 0.6 and 1.2 eV by integrating the signal under the elastic energy-loss peaks in NO and in He. The energy-loss peaks were similar to those in to the topmost spectrum in figure 1, the spin-orbit transitions are relatively weak at these three energies. Their contributions were determined by fitting three empirical Gaussian profiles under the superelastic, elastic, and inelastic signals in the energy-loss spectra. Only the (rotationally averaged) elastic cross sections, with the spin-orbit inelastic and superelastic contributions subtracted, are given in table 1. This data is thus not directly comparable with data from lower resolution experiments, which integrate both over the rotational and the spin-orbit transitions. In the previous paper [3] the contributions of the spin-orbit inelastic and superelastic transitions were neglected and not subtracted when determining the absolute elastic values at the three discrete energies. The present cross sections, with the contributions of the spin-orbit transitions subtracted, are consequently somewhat lower than those given earlier [3].

An excitation function was then recorded at the energy-loss $\Delta E = 0$ eV, corrected for the instrumental response function determined on the elastic scattering in helium and normalized to the absolute value at 0.2 eV. The absolute elastic measurements at discrete energies are more reliable (within about ± 15 %) than the values obtained from the excitation function. The excitation function normalized at 0.2 eV therefore does not automatically agree perfectly with the discrete absolute measurements at 0.6 and 1.2 eV. In the present work the response function was slightly adjusted to improve the fit to the absolute measurements at discrete energies and the shape of the cross section is not exactly the same as in the earlier publication [3]. The elastic excitation function normalized in this way is given in the bottom trace of figure 2 and, on a horizontally expanded scale, figure 3.

As mentioned above, the measured elastic signal is a superposition of elastic scattering on both thermally populated spin-orbit states. The two contributions can be distinguished near a resonance because the narrow resonant features occur at different energies as has been described previously [3] and as shown in figure 4. The present absolute values are slightly lower than those given in reference [3] for the reasons given above. As pointed out earlier [3], the elastic cross section for the $\Omega = 3/2$ state is, somewhat surprisingly, measured to be smaller than that of the $\Omega = 1/2$ state.

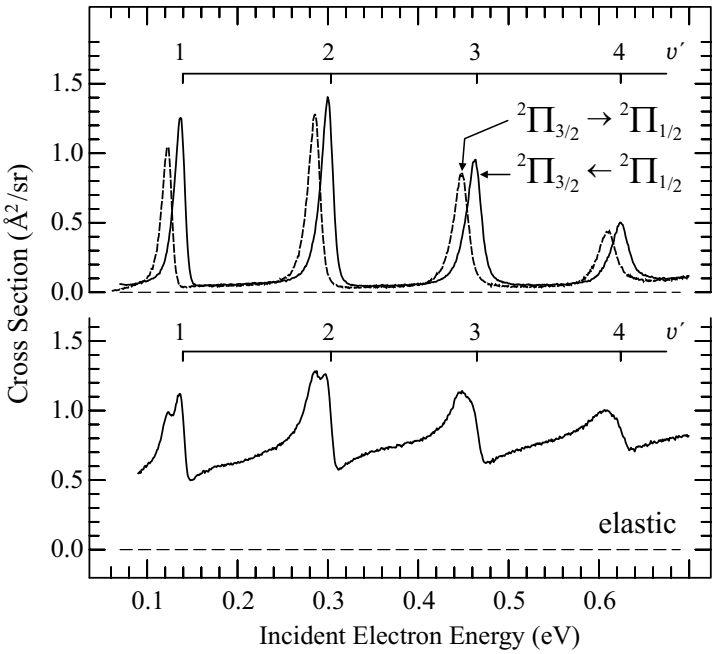

Figure 3. Expanded view of the differential elastic cross section $\langle\sigma_{\Delta\Omega=0}\rangle$ (bottom), and the cross sections inelastic and superelastic with respect to the electronic fine structure transition, $\sigma_{\Delta\Omega=+1}$ and $\sigma_{\Delta\Omega=-1}$, respectively. The scattering angle was $\theta = 135°$.

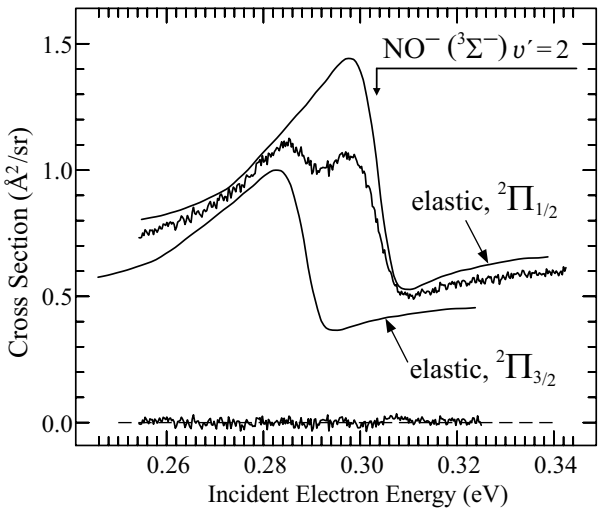

Figure 4. Detail of the elastic cross section. The scattering angle was $\theta = 135°$. The smooth lines are the elastic cross sections for NO in the $\Omega = 1/2$ and $\Omega = 3/2$ states, $\sigma_{\Omega=1/2\rightarrow1/2}$ and $\sigma_{\Omega=3/2\rightarrow3/2}$, respectively, obtained by deconvolution of the data as explained in reference [3]. The line at the bottom shows the residuals of the fit.

Table 2. Parameters of the NO^- resonances. The origin refers to the lowest ro-vibrational level in the present work.

state	source	origin (meV)	$\tilde{\nu}_e$ (cm^{-1})	$\tilde{\nu}_e x_e$ (cm^{-1})
$^3\Sigma^-$	present	-26.8	1360	9.5
	Tronc *et al* [10]	-50	1363	8
	Alle *et al* [14]	-33	1371	8
$^1\Delta$	present	740	1480	8
	Tronc *et al* [10]	750	1492	(8)

The spin-orbit inelastic and superelastic excitation functions were recorded at the fixed energy-loss and energy-gain of 15 meV, respectively. These excitation functions were then normalized to reflect the areas (not the heights) under the inelastic ($\Omega = 1/2 \rightarrow 3/2$) and the superelastic ($\Omega = 3/2 \rightarrow 1/2$) bands in figure 1, fitted by Gaussian profiles. The inelastic and the superelastic bands were found to be wider (16.5 meV) than the elastic band (8.5 meV), indicating a higher degree of rotational excitation. The excitation functions were subsequently divided by the thermal populations of the initial levels to yield the cross sections $\sigma_{\Delta\Omega=+1}$ and $\sigma_{\Delta\Omega=-1}$. They are shown in figures 2 and 3. The cross sections for the fine structure transitions are unusually large for an electronic transition – the peak inelastic cross sections in figure 2 is higher than the peak elastic cross section! (This reflects the fact that the inelastic energy-loss band is broader than the elastic peak, leading to a larger area. The inelastic band is not higher.) The very large cross sections can be understood qualitatively in terms of resonance parentage [3]. The situation is related [3] to that found for resonant excitation of the $a^1\Delta$ state in O_2 [27], with the difference that in NO the final electronic state is energetically below the vibrational levels of the resonance whereas in O_2 it lies above.

The elastic cross section consists of a continuous background with superimposed narrow resonant structures. The two components interfere coherently and the structures have the shapes of Fano profiles, with a shallow dip on the high energy side of each peak (figure 3). In contrast, the cross sections for the spin-orbit transitions have only very weak nonresonant background and are dominated by the resonance contribution. Note that the 'elastic' cross sections in earlier work [10, 16, 13] are integrated over the $\Delta\Omega = 0, \pm 1$ transitions, and the resonant peaks appear higher relative to nonresonant background there than in the present 'pure' elastic cross section.

In the elastic and even more in the spin-orbit inelastic cross section two progressions distinguishable by substantially different peak widths can be discerned (figure 2). The widths in the first progression are 15-20 meV, increasing with energy, in the second progression around 80 meV. The lowest peak of the second progression is at 0.74 eV and marks its origin. The same conclusion was reached by a more complex analysis of lower resolution data by Tronc *et al* [10] and Teillet-Billy and Fiquet-Fayard [11] and later by Alle *et al* [14] and Buckman *et al* [15]. The parameters and the well known assignments of the two progressions are given in table 2. The value of the electron affinity

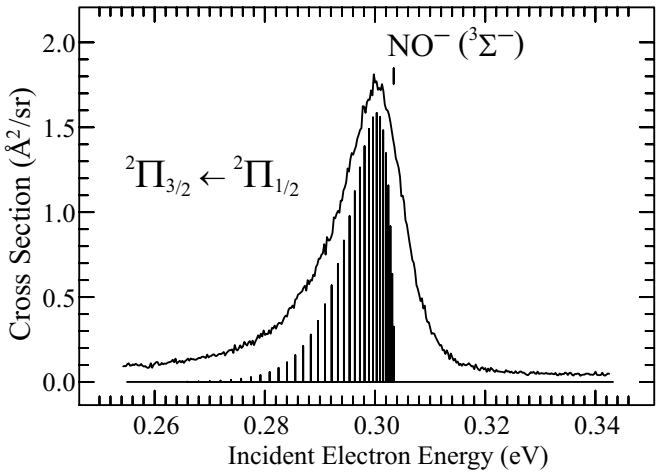

Figure 5. Detail of the inelastic cross section $\sigma_{\Delta\Omega=+1}$ around the $v' = 2$ level of the NO^- $^3\Sigma^-$ resonance. The expected energies of the $\Delta N = 0$ rotational transitions (NO $^2\Pi_{1/2}$ $v = 0 \rightarrow NO^-$ $^3\Sigma^-$ $v' = 2$) are indicated. The scattering angle was $\theta = 135°$.

is in a fortuitously good agreement with the (rotationally adjusted) photoelectron value of 0.026 ± 0.005 eV [22]. Note that the present energies are taken at the presumed band origin, slightly to the right of the peak maxima, as suggested by the rotational profile in Fig. 5. That means that they are also rotationally adjusted. The resonance parameters are in excellent agreement with those derived by Tronc *et al* [10], the improved resolution of the present experiment did not lead to substantial improvement of the parameters. The difference of electron affinities is presumably, at least in part, due to the fact that their value refers to band maximum, whereas the present value (and the electron affinity value of reference [22]) refer to band origins. The resonance energies are also in good agreement with other earlier measurements [8, 16].

The peaks in the inelastic and superelastic cross sections in figure 3 are asymmetrical, and the $v' = 2$ peak, recorded with a slightly higher resolution, is shown in more detail in Fig. 5. The envelope of the $\Delta N = 0$ transitions indicates that the asymmetry is primarily caused by unresolved rotational structure. The rotational width is relatively large, about 9 meV for the $\Delta N = 0$ transitions shown, because the internuclear separations r_e and consequently the rotational constants B_e of NO and NO^- are quite different [2]. In reality the transitions with $\Delta N = \pm 1$ and ± 2 probably also contribute and make the rotational profile even wider. The width of the experimental band at half height (fwhm) in Fig. 5 ($v' = 2$) is 13.5 meV. Subtracting (taking the root of the difference of the squares) the contributions of the estimated instrumental (7 meV) and $\Delta N = 0$ rotational (9 meV) widths leads to an estimate of the upper limit of the autodetachment width of the NO^- $^3\Sigma^-$ $v' = 2$ resonance to be about 7 meV. This is narrower than reported previously, the narrowest width reported for the $v' = 2$ level was 29 meV [16]. The present value is, however, in a remarkably good agreement with the value of 5 meV calculated by Teillet-Billy and Fiquet-Fayard [11] within their

model from the absolute cross section values. Note that the cross section measured in reference [16] was a superposition of the elastic and electronically inelastic cross sections because the final states were not resolved. On the other hand their spectrum was not rotationally broadened because of supersonic expansion cooling of the sample.

Because of the microscopic reversibility principle the superelastic cross section would be expected to be about equal, at low energies even somewhat larger than the inelastic cross section. The superelastic cross sections figure 3 are slightly lower than the inelastic peaks. This result is not significant, however, the difference could be the consequence of a small error in the fitting of the data into Gaussian profiles, or to a weak cooling of the sample in the present, nominally effusive nozzle. The mean free path of the NO molecules at the high pressure side of the nozzle, (about 80 μm at 1.1 mbars, assuming that the molecule is a sphere with 4 Å diameter) is slightly shorter than the nozzle diameter (250 μm), allowing for a few collisions. The spin-orbit states have been found to be cooled very efficiently in an expansion, nearly as efficiently as rotation [26].

Mojarrabi *et al* [12] reported the value of 0.75 $\pm$ 6.5 % Å^2/sr for the elastic cross section at 1.5 eV and 130°. They have also shown that the angular dependence is flat around 130° at 1.5 eV so that their value can be compared to the present value at 135°. They used a resolution of $40 - 60$ meV and their data is consequently summed over the spin-orbit transitions. The corresponding sum, averaged over thermal populations, can be obtained from the present data as $\langle\sigma_{\Delta\Omega=0,\pm1}\rangle = \langle\sigma_{\Delta\Omega=0}\rangle + 0.64 \cdot \sigma_{\Delta\Omega=+1} + 0.36 \cdot \sigma_{\Delta\Omega=-1} = 0.76 + 0.64 \cdot 0.22 + 0.36 \cdot 0.21 = 0.98$ Å^2/sr ($\pm$25 %) (where the angle bracket means averaged over thermal populations of target states). This is higher than the value of Mojarrabi *et al*, but within the combined confidence limits of the two experiments.

Figure 6 shows two vibrational excitation cross sections. The pure vibrational cross section in the bottom of the figure is, similarly to the elastic cross section, an average of the two transitions ($\Omega = 1/2 \rightarrow 1/2$ and $3/2 \rightarrow 3/2$), elastic with respect to the electronic fine structure, weighted by the thermal populations of the initial states. The resonant peaks could be expected to be doublets, for the same reason as in the elastic cross section in figures 3 and 4. The doubling is less clear here, because the narrow low-lying resonance levels for which clear double peak was visible in the elastic cross section ($v' = 1$ and 2) are not visible or are only weak in the VE cross section. But the $v' = 2$, 3 and 4 peaks in figures 6 and 7 are clearly broader in the pure VE curve than in the VE+($\Omega = 1/2 \rightarrow 3/2$) cross section, indicating that they do consist of two bands.

Both the pure vibrational and the vibrational plus electronic excitation cross sections have essentially the same shape. The shape appears to be determined by nuclear dynamics which is not affected by the electronic part of the transition. The peaks in the $\Delta\Omega = -1$ cross section are, as expected, shifted to lower energies in figure 7. They are slightly smaller than those in the inelastic cross section and the same remark applies as made above for the purely electronic transitions. The difference is not truly significant and could be due to imperfection of the fitting of the rotational profiles to Gaussian functions or to a slight expansion cooling of the sample.

Figure 8 shows cross sections summed over all $\Delta\Omega$ transitions. The $v = 0 \rightarrow 0$ and

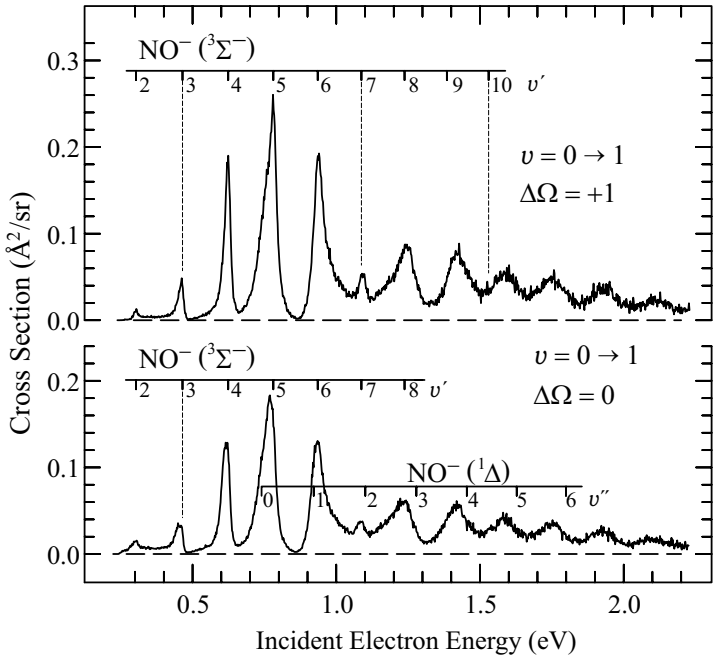

Figure 6. Cross sections for exciting $v = 1$. The lower curve is $\langle \sigma^{v=0\to1}_{\Delta\Omega=0} \rangle$, a superposition of scattering on the $\Omega = 1/2$ and $\Omega = 3/2$ initial states, weighted by their thermal population in the sample. The upper curve is $\sigma^{v=0\to1}_{\Delta\Omega=+1}$. The scattering angle was $\theta = 135°$.

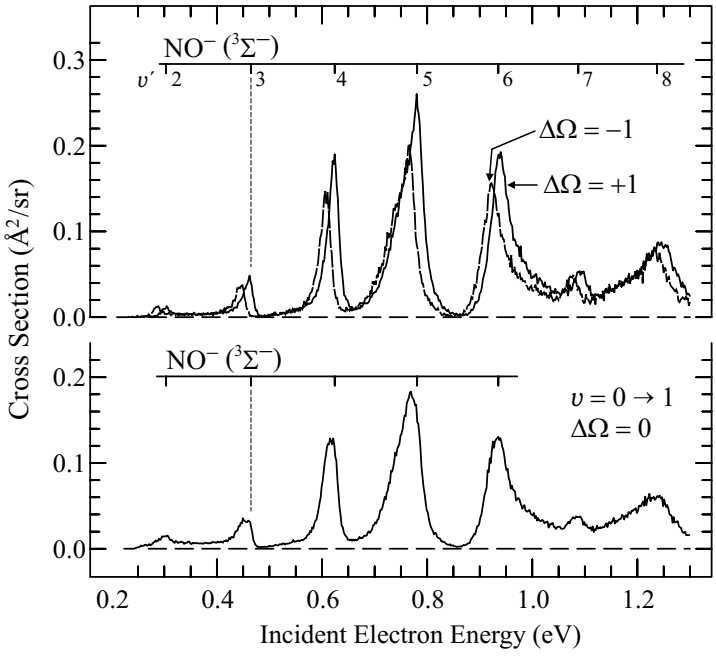

Figure 7. Cross sections for exciting $v = 1$. The lower curve is $\langle \sigma^{v=0\to1}_{\Delta\Omega=0} \rangle$, as in figure 6. The upper curves are $\sigma^{v=0\to1}_{\Delta\Omega=+1}$ and $\sigma^{v=0\to1}_{\Delta\Omega=-1}$ (dashed). The scattering angle was $\theta = 135°$.

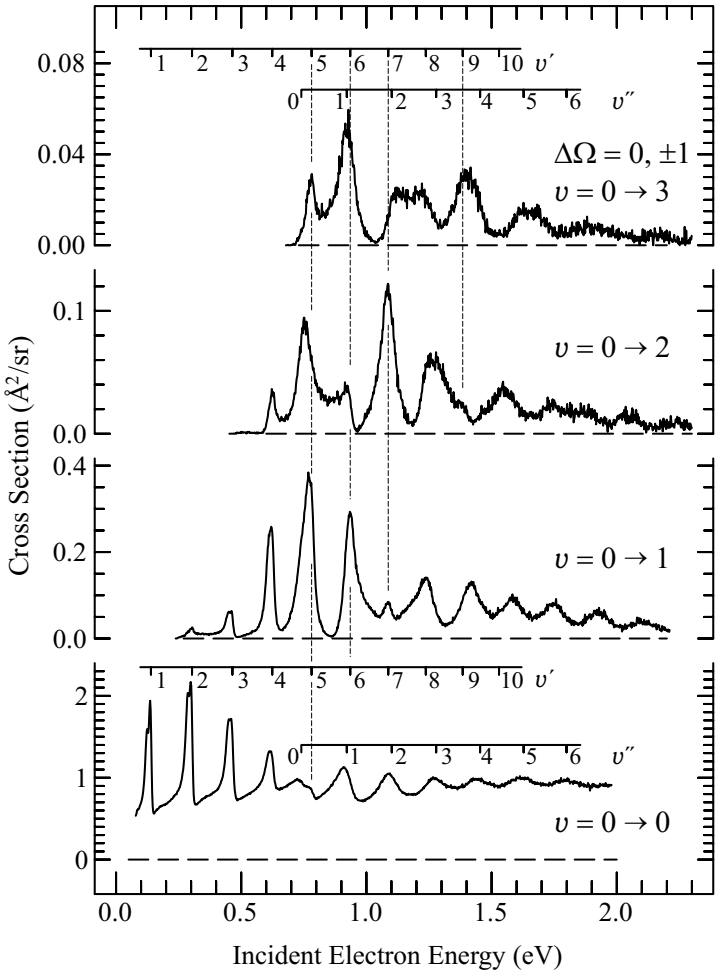

Figure 8. Elastic cross section and cross sections for exciting $v = 1$, 2 and 3, all summed over the $\Delta\Omega = 0, \pm 1$ transitions and averaged over the thermal populations. The scattering angle was $\theta = 135°$.

$v = 0 \rightarrow 1$ cross sections are the sums of the $\Delta\Omega = 0, \pm 1$ cross sections from figures 3 and 7, weighted by the thermal populations of the initial states. The magnitudes can thus be compared to the results of lower resolution experiments. The cross sections for the $v = 0 \rightarrow 2$ and 3 transitions were recorded at energy-losses corresponding to the electronically elastic, pure vibrational transitions, but were normalized to reflect the spin-orbit integrated transitions. This is justified since, as figures 6 and 7 demonstrate, an accompanying electronic transition does not change the shape of the cross section except for a 15 meV shift of the resonant peaks.

The shapes of the resonant peaks in all curves in figure 8 are very peculiar. Many peaks are asymmetrical, they are shaded towards lower or higher energies. In the $v = 0 \rightarrow 1$ cross section, shown in more detail in figure 7, the $v' = 4$ and 5 peaks are shaded toward lower energies, the $v' = 6$ peak toward higher energies, the $v' = 7$ peak is narrow without apparent shading and the $v' = 8$ is shaded toward lower energies. As a consequence, the valleys between peaks are sometimes very deep, with cross section

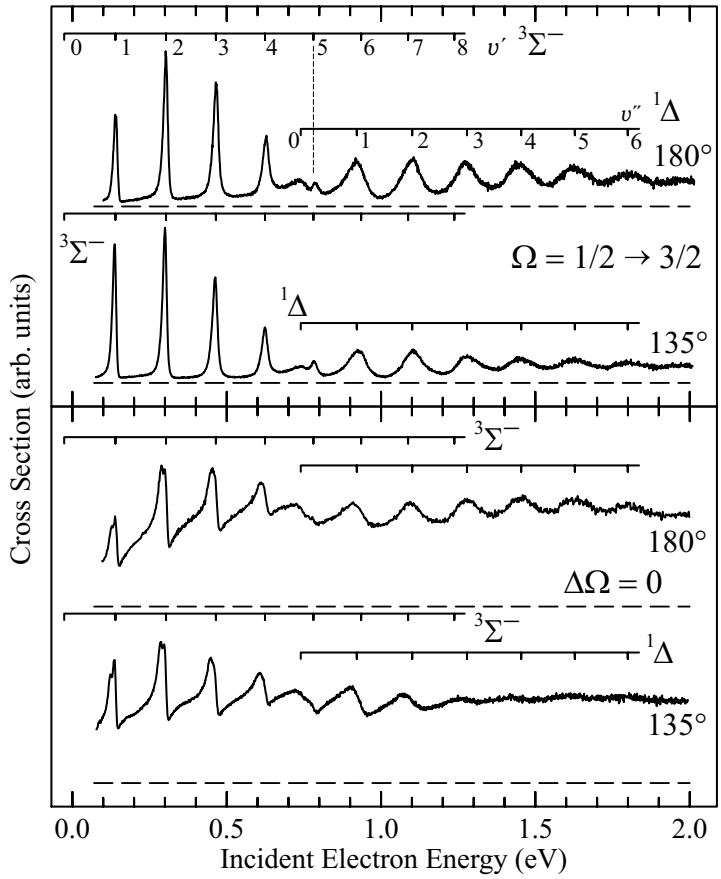

Figure 9. Elastic sections (bottom two spectra) and cross section for exciting the $\Omega = 3/2 \rightarrow 1/2$ transition (top two spectra) at the scattering angles $\theta = 135°$ and $\theta = 180°$.

dropping to nearly zero, such as between $v' = 5$ and $v' = 6$ in the $v = 0 \rightarrow 1$ cross section or the $v' = 6$ and $v' = 7$ in the $v = 0 \rightarrow 3$ cross section, and are nearly missing at other times, for example between the $v' = 7$ and $v' = 8$ peaks in the $v = 0 \rightarrow 3$ cross section. The spacings between the peaks at higher energies and higher channels are not regular and the peak positions are not the same in the elastic and the various inelastic channels. The peak heights are irregular as well. The irregularities make it difficult to assign individual peaks to individual resonances at higher energies. These phenomena were already observed, at lower resolution, by Tronc *et al* [10] in the cross sections measured at 40°. The irregularities are caused in part by the overlap of the structures belonging to the $^3\Sigma^-$ and $^1\Delta$ resonances, but primarily to the autodetachment width of the resonances and the resulting boomerang-like motion of the nuclei. Teillet-Billy and Fiquet-Fayard [11, 28] calculated the cross section for the $v = 0 \rightarrow 1$ transition *via* the $^1\Delta$ resonance and obtained, qualitatively correctly, the irregularities. Their calculated $v = 0 \rightarrow 1$ cross section *via* the $^1\Delta$ resonance exhibits the 'shading' of the bands and the deep and missing valleys, and is in these respects reminiscent of the cross sections in figure 8, in particular the $v = 0 \rightarrow 3$ cross section. Note that the

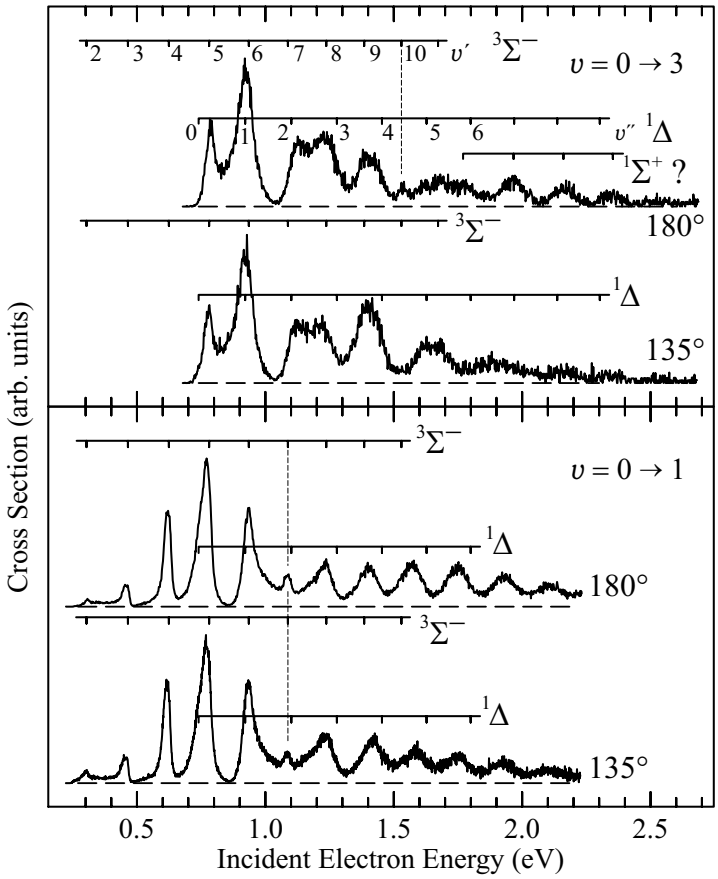

Figure 10. Cross sections for exciting $v = 1$ and 3 at the scattering angles $\theta = 135°$ and $\theta = 180°$.

contributions of the $^3\Sigma^-$ and $^1\Delta$ states to the cross sections are strictly additive and do not involve interference terms [11, 20], the irregularities are not a consequence of interference between the resonances.

A very coarse estimate of the integral cross section, obtained by multiplying the present differential cross section by 4π, yields a peak elastic cross section of 26 Å^2, which compares favorably with the calculated value of Zhang *et al* [20]. An estimate of the peak $v = 0 \rightarrow 1$ cross section yields 4.6 Å^2 at 0.77 eV, which compares favorably with the values proposed by Josić *et al* [17] and calculated by Zhang *et al* [20], but is higher than the value of Jelisavcić *et al* [13].

An attempt was made to identify the third resonance, $^1\Sigma^+$, by recording spectra at a different angle. Figure 9 compares the elastic and the spin-orbit inelastic cross sections at 135° and 180°. The elastic cross sections are very similar up to an energy of about 1 eV, but the boomerang structure is more pronounced at 180° above 1 eV. Similar observation is made also for the $\Omega = 1/2 \rightarrow 3/2$ transition. The positions of the peaks do not change, however, all peaks observed at 180° fit either the $^3\Sigma^-$ or the $^1\Delta$ transitions. The observations thus do not permit an unambiguous identification of the $^1\Sigma^+$ resonance.

Figure 10 compares the vibrational excitation cross sections. Again, the oscillatory structure at higher energies is more pronounced at 180°. The broad peaks do not fit the $^1\Delta$ vibrational grid derived on the elastic and spin-orbit inelastic cross sections, but this is not surprising since a dependence of the peak energies on the final channel must be expected for boomerang structure. The more pronounced peaks in the $v = 0 \rightarrow 3$ channel could stem from the $^1\Sigma^+$ resonance. The spectra do not permit the identification of the origin of this progression, however. Somewhat surprisingly, a weak narrow peak fitting the $v' = 10$ level of the $^3\Sigma^-$ resonance appears in the $v = 0 \rightarrow 3$ cross section at 180°.

4. Conclusions

Absolute elastic, electronic fine structure and vibrational excitation cross sections have been measured at 135°. The cross sections for the change of Ω have been found to be dominated by resonances, with very little direct contribution. They have been found to be very large, having about the same magnitude as the cross sections with $\Delta\Omega = 0$, both for the vibrationally elastic and vibrationally inelastic collisions. This fact can be qualitatively understood in terms of resonance parentage. Both spin-orbit states are parent states of both the $^3\Sigma^-$ and the $^1\Delta$ resonances, both are energetically accessible, so that it is not surprising that the resonances decay into both with about equal probabilities. The autodetachment width of the $^3\Sigma^-$ resonance has been found narrower than reported previously, with an upper limit of about 7 meV for the $v' = 2$ level. The vibrational cross sections have peculiar shapes, in particular in the region of the $^1\Delta$ resonance. The shapes of the structures depend on the final channel. The structures are often asymmetric, shaded sometimes toward higher, sometimes toward lower energies. The valleys between the structures have widely varying depths. While such phenomena can be expected for boomerang structure, the irregularities are more complex than, for example, for the $^2\Pi_g$ resonance in N_2. Relative cross sections have been also measured at 180° and reveal dependence of relative intensities of the resonant structures above 1.6 eV on scattering angle.

Acknowledgments

This research is part of project No. 200020-105226/1 of the Swiss National Science Foundation.

References

[1] Herzberg G 1950 *Molecular Spectra and Molecular Structure, Vol. I. Spectra of Diatomic Molecules* (N. Y.: Van Nostrand Reinhold Company) p 212

[2] Huber K P and Herzberg G 1979 *Molecular Spectra and Molecular Structure, Vol. IV. Constants of Diatomic Molecules* (N. Y.: Van Nostrand Reinhold Company) pp 484 & 486

[3] Allan M 2004 *Phys. Rev. Lett.* **93** 063201

[4] Allan M 2001 *Phys. Rev. Lett.* **87** 033201
[5] Ehrhardt H and Willmann K 1967 *Z. Phys.* **204** 462
[6] Boness M J W, Hasted J B and Larkin I W 1968 *Proc. Roy. Soc. (London)* A **305** 493
[7] Spence D and Schulz G J 1971 *Phys. Rev.* A **3** 1968
[8] Burrow P D 1974 *Chem. Phys. Lett.* **26** 265
[9] Zecca A, Lazzizzera I, Kraus M and Kuyatt C E 1974 *J. Chem. Phys.* **61** 4560
[10] Tronc M, Huetz A, Landau M, Pichou F and Reinhardt J 1975 *J. Phys. B: At. Mol. Phys.* **8** 1160
[11] Teillet-Billy D and Fiquet-Fayard F 1977 *J. Phys. B: At. Mol. Phys.* **10** L111
[12] Mojarrabi B, Gulley R J, Middleton A G, Cartwright D C, Teubner P J O, Buckman S J and Brunger M J 1995 *J. Phys. B: At. Mol. Opt. Phys.* **28** 487
[13] Jelisavcić M, Panajotović R and Buckman S J 2003 *Phys. Rev. Lett.* **90** 203201
[14] Alle D T, Brennan M J and Buckman S J 1996 *J. Phys. B: At. Mol. Opt. Phys.* **29** L277
[15] Buckman S J, Alle D T, Brennan M J, Burrow P D, Gibson J C, Gulley R J, Jacka M, Newman D S, Rau A R P, Sullivan J P and Trantham K W 1999 *Aust. J. Phys.* **52** 473
[16] Randell J, Lunt S L, Mrotzek G, Field D and Ziesel J P 1996 *Chem. Phys. Lett.* **252** 253
[17] Josić L, Wróblewski T, Petrović Z L, Mechlińska-Drewko J and Karwasz G P 2001 *Chem. Phys. Lett.* **350** 318
[18] Zecca A, Karwasz G P, Brusa R S and Wróblewski T 2003 *Int. J. Mass. Spectr.* **223-224** 205
[19] Tennyson J and Noble C J 1986 *J. Phys. B: At. Mol. Phys.* **19** 4025
[20] Zhang Z, Vanroose W, McCurdy C W, Orel A E and Rescigno T N 2004 *Phys. Rev.* A **69** 062711
[21] Siegel M W, Celotta R J, Hall J L, Levine J and Bennett R A 1972 *Phys. Rev.* A **6** 607
[22] Travers M J, Cowles D C and Ellison G B 1989 *Chem. Phys. Lett.* **164** 449
[23] Allan M 1995 *J. Phys. B: At. Mol. Opt. Phys.* **28** 5163
[24] Gopalan A, Bömmels J, Götte S, Landwehr A, Franz K, Ruf M W, Hotop H and Bartschat K 2003 *Eur. Phys. J.* D **22** 17
[25] Nesbet R K 1979 *Phys. Rev.* A **20** 58
[26] Amrein A, Quack M and Schmitt U 1988 *J. Phys. Chem.* **92** 5455
[27] Teillet-Billy D, Malegat L and Gauyacq J P 1987 *J. Phys. B: At. Mol. Phys.* **20** 3201
[28] Fiquet-Fayard F 1975 *J. Phys. B: At. Mol. Phys.* **8** 2880